2018

Atomistic Simulation of the Interaction Between Point Defects and Twin Boundary

Liang Zhang
University of Tokyo

Yasushi Shibuta
University of Tokyo

Cheng Lu
University of Wollongong, chenglu@uow.edu.au

Xiaoxu Huang
Chongqing University

Atomistic Simulation of the Interaction Between Point Defects and Twin Boundary

Abstract

While nanotwinned metals have been proven to show excellent mechanical properties, they are generally anticipated to be less effective in the alleviation of radiation damage. However, recent in situ studies have indicated that some nanotwinned metals exhibit unprecedented radiation tolerance, and the unexpected self-healing of twin boundaries in response to radiation was observed. To reveal the underlying atomic mechanisms, we performed long-time molecular dynamics simulations to study the dynamic interaction between twin boundary and some typical radiation-induced point defects, including vacancy cluster and self-interstitial atoms. The defective structures of coherent twin boundary which contains incoherent twin segment or self-interstitial atoms are considered, and these structure features are found to effectively improve the ability of twin boundary to act as a sink for point defects.

Disciplines

Engineering | Science and Technology Studies

Publication Details

Zhang, L., Shibuta, Y., Lu, C. & Huang, X. (2018). Atomistic Simulation of the Interaction Between Point Defects and Twin Boundary. Physica Status Solidi B: Basic Solid State Physics, 255 (9), 1800228-1-1800228-9.

Atomistic simulation of the interaction between point defects and twin boundary

Liang Zhang [a,*], Yasushi Shibuta [a], Cheng Lu [b], Xiaoxu Huang [c]

[a] Department of Materials Engineering, The University of Tokyo, Bunkyo-ku, Tokyo 113-8656, Japan

[b] School of Mechanical, Materials and Mechatronic Engineering, University of Wollongong, Wollongong, NSW 2522, Australia

[c] School of Materials Science and Engineering, Chongqing University, Chongqing, 400044, China

* Corresponding author. E-mail: liang@mse.mm.t.u-tokyo.ac.jp (L. Zhang)

Abstract: While nanotwinned metals have been proven to show excellent mechanical properties, they are generally anticipated to be less effective in the alleviation of radiation damage. However, recent *in situ* studies have indicated that some nanotwinned metals exhibit unprecedented radiation tolerance, and the unexpected self-healing of twin boundaries in response to radiation was observed. To reveal the underlying atomic mechanisms, we performed longtime molecular dynamics simulations to study the dynamic interaction between twin boundary and some typical radiation-induced point defects, including vacancy cluster and self-interstitial atoms. The defective structures of coherent twin boundary which contains incoherent twin segment or self-interstitial atoms were considered, and these structural features were found to effectively improve the ability of twin boundary to act as a sink for point defects.

Keywords: twin boundary; vacancy cluster; interstitial atom; molecular dynamics

1. Introduction

There is increasing interest in nanostructured metallic materials because they possess a significant fraction of grain boundaries leading to excellent properties compared with their coarse-grained counterparts [1-3]. For example, the well-known nanotwinned metals have shown an improved strength and ductility, yet maintain high electrical conductivity and good thermal stability [4-6]. However, it was considered that they do not have high radiation resistance because they contain mostly coherent twin boundaries (CTBs), which are low-energy boundaries and are inefficient defect sinks in irradiated metallic materials [7, 8]. The low ability of CTBs to act as sinks for radiation-induced defects has also been verified on the basis of computational simulations [9, 10]. However, some recent *in situ* studies revealed that twin boundaries can also show outstanding capability to act as sinks in irradiated nanotwinned metals [11]. Yu et al. [12] observed that a large number of radiation-induced stacking fault tetrahedra (SFTs) were removed during their interactions with abundant twin boundaries in nanotwinned Ag. Chen et al. [13] found that nanotwinned Cu exhibited a smaller defect size and lower defect density than its coarse-grained counterpart under irradiation. Moreover, the twin boundary affected zone and the self-healing capability of twin

boundaries in response to irradiation have been observed in nanotwinned Cu [14] and nanotwinned Ag [15]. The above experimental findings go against the conventional understanding of nanotwinned materials, which have long been considered as being ineffective for the alleviation of radiation damage. To reveal the underlying mechanisms, we studied the dynamic interaction between twin boundaries and some typical radiation-induced point defects by molecular dynamics (MD) simulations.

Existing simulation models typically used in MD simulations generally assume perfect Σ3{111} CTBs to study their mechanical and physical properties [16-18] and their interaction with other types of crystal defects (e.g., vacancies, interstitials, SFTs, and dislocation loops) [7, 10, 19]. These studies are informative as long as CTB lengths are limited to 10 nm order. However, the much longer CTBs usually observed in experiments are inherently defective with kink-like steps, which consist of segments of Σ3{112} incoherent twin boundaries (ITBs) and partial dislocations [20, 21]. Moreover, nanotwinned structures are not as stable as they were thought be. Both experimental and simulation studies have shown that an ITB in the junction of {111}/{112}/{111} twins can migrate accompanied by the detwinning of CTBs during annealing [22, 23], under an externally applied mechanical load [24] or under irradiation [12, 25]. On the other hand, the initial radiation cascades near a grain boundary can play a significant role in changing the local boundary structure since self-interstitial atoms (SIAs) resulting from the radiation can be easily absorbed by the nearby boundaries [26-28]. Therefore, it is expected that the perfect CTB structure may be changed by radiation-induced SIAs. For example, the frequent distortion of CTBs in irradiated nanotwinned Ag observed by Li et al. [15] may confirm this hypothesis. As discussed above, the generally assumed perfect CTBs may usually have imperfect structures in real materials that either contain incoherent twin segments or are incorporated with point defects under irradiation conditions. On the basis of recent experimental findings, it is conceivable that these structural features are closely related to the ability of twin boundaries to act as a sink for radiation-induced defects, and they are expected to affect the overall radiation tolerance of nanotwinned materials. Neverthless, the ability of defective CTBs to act as a sink has not been studied so far and the underlying mechanisms are not clear. In this study, we carried out long-time MD simulations (100 ns time scale) to provide further information at the atomic scale.

2. Simulation method

The simulations were conducted using the parallel molecular dynamics code LAMMPS [29] with the embedded-atom method (EAM) potential for Cu [30]. In the first study, we investigated the effect of the CTB/ITB structure on the stability of radiation-induced defects, as illustrated in Fig.1(a). To simulate the junction of {111}CTB and {112}ITB, a rectangular simulation box (region I) with Cu atoms was first constructed along the $[\bar{1}12]$, $[1\bar{1}1]$ and

[110] directions, and then followed by a grain rotation about the [110] axis in region II. The coordinate axis for the crystal and twinned regions are indicated in Fig.1(a). The SFT was chosen for study because it is an important type of vacancy cluster in various irradiated face-centered cubic (fcc) metals [31, 32]. Following the previous method [33], the initial SFT structure was created from an equilateral triangle vacancy plate on the basis of the Silcox—Hirsch mechanism. Three SFTs (SFT-1 to SFT-3) with various distances to the twin boundaries were introduced into the CTB/ITB region. In the simulation, the sample was first subjected to an energy minimization procedure by the conjugate gradient algorithm. Then, the sample was heated to 1000 K in the canonical (NVT) ensemble using a constant temperature Nose-Hoover thermostat. During the system annealing at the high temperature, a thin slab of atoms on the left and right sides of the sample was fixed, while all the other atoms were set as free. Fig.2 shows the atomic structure of CTB/ITB junctions after the initial system minimization procedure. The structure of ITB can be presented as a line of rhombic structural units (SUs) and a group of stacking faults that dissociated from the boundary plane, as outlined by the yellow lines. From the perspective of dislocation, the {112}ITB consists of a set of Shockley partial dislocations on every {111} plane with a repeatable sequence b_1:b_2:b_3 [24]. The structures of ITB and the CTB/ITB junctions constructed in this study are consistent with the experimental observations by using the high-resolution transmission electron microscopy (HRTEM) [22, 34].

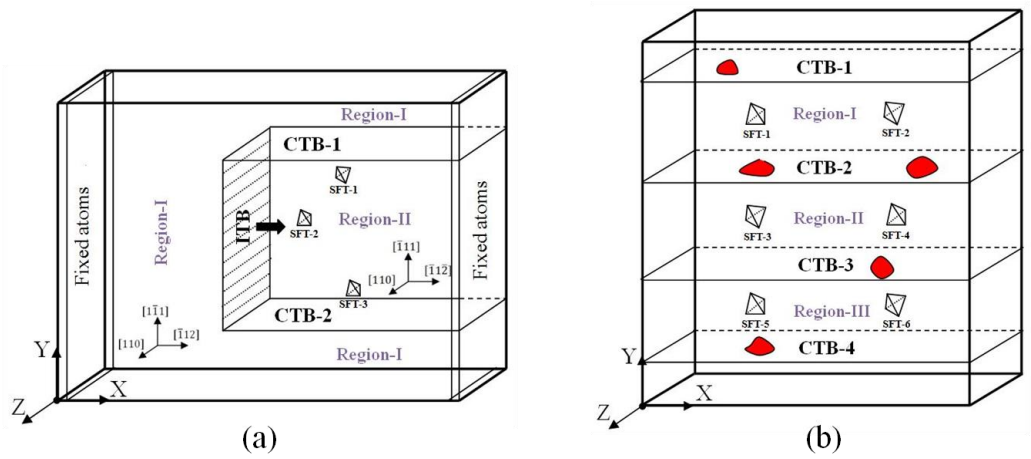

Figure 1 Schematic of the simulation models. (a) Coherent twin boundary (CTB) with incoherent twin boundary (ITB) segment. (b) Nanotwinned structure with defective coherent twin boundaries. The areas colored in red represent the local defective structure of the CTBs after incorporating the interstitial atoms.

In the second study, we examined the effect of interstitial atoms on the structure of CTBs and the ability of the defective CTBs to act as a sink for the vacancy clusters, as shown in Fig.1(b). A nanotwinned Cu sample containing

four CTBs was constructed, and then SFTs and SIAs were introduced into the sample respectively. The size of the simulation sample in Y direction is about 250 Å, so the separation between the CTBs is 62.5 Å. Again, the simulation sample was heated to 1000 K, and MD simulations were performed in the NVT ensemble with all the atoms set free. Note that, the mobility of the SFT decreases exponentially fast with increasing SFT size. It was reported that the mobility of a 15-V SFT (an SFT created from 15 vacancies) is negligible on the time scale of MD simulations, but a 10-V SFT has much higher mobility than the 15-V SFT [35]. Therefore, all the SFTs introduced in this study were created from 10 vacancies to ensure a sufficient mobility of the SFTs in an appropriate simulation time.

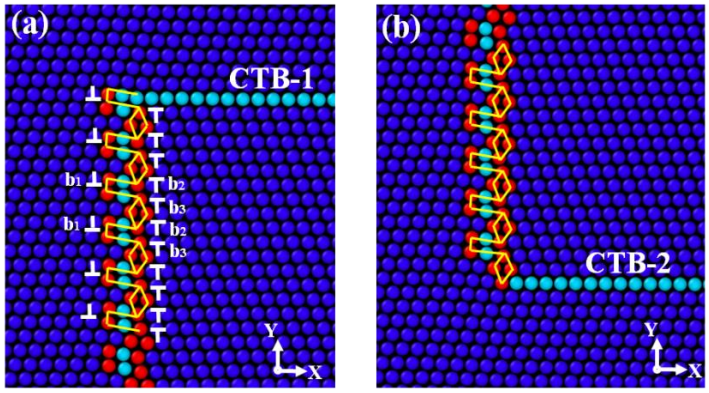

Figure 2 Atomic structure of the junctions between (a) CTB-1 and ITB, (b) CTB-2 and ITB. Atoms are colored according to their common neighbor analysis (CAN) values, where the dark blue atoms have perfect fcc structure, and the atoms of CTB and ITB are expressed by light blue and red. The yellow lines outlined the ITB structure.

3. Result and discussion

3.1 Migration of ITB

We first investigate the size effect and the effect of temperature on the mobility of CTB/ITB junction. CTB/ITB junction is a high-energy configuration and the motion of an ITB can be induced under various circumstances. Here, the migration of an ITB and the corresponding detwinning of CTBs are thermally activated processes at a high temperature. During the migration of the ITB, the length of the two CTBs decreased and the Gibbs free energy of the system was thereby lowered. To determine the size effect, we simulated the migration process of the CTB/ITB junction with a CTB distances of 4, 6, 8, and 10 SUs. The number of SUs corresponds to a ITB length of 25 Å, 37.6 Å, 50 Å, and 62.6 Å, respectively. The thickness of the twin boundaries (in Z direction) was set as 20.4 Å. The snapshots in Fig.3(a) and (b) show the configurations of the ITB with 4 SUs and 10 SUs after the system was annealed at 900 K for 10 ns and 40 ns, respectively. Fig.4(a) shows the migration distance of the ITB as a function of the simulation time, where the migration velocity was obtained by least-squares fitting. It was found that the longer the boundaries, the slower the boundary migration. The reduction of the velocity was found to be less significant upon

further increasing the length of the ITB, which may owing to the size of the simulation sample in Y direction and the periodic boundary condition applied in this direction. Moreover, the thermally activated migration of the ITB was correlated to the collective motion of boundary atoms which was sensitive to the temperature. The snapshots in Fig.3(c) and (d) show the configurations of the ITB with 24 SUs after 40 ns simulation at 700 K and 1000 K, respectively. Fig.4(b) plots the migration distance of the ITBs as a function of the simulation time at different temperatures. From the above results, it was concluded that the migration velocity of the ITB increases monotonically with the temperature but decreases with increasing length of the ITB. The results are qualitatively consistent with the experimental observations in twin boundaries of nanocrystalline Cu [22]. When SFTs were introduced to the sample, we doubled the thickness of the twin boundaries to 40.8 Å to ensure a sufficient interaction between the twin boundaries and the SFTs. Simulations showed that the increase in size of the thickness further decreased the migration velocity of the ITB. By considering the time-scale limitation of MD simulations, we constructed the ITB with a suitable size and carried out the simulation at a relatively high temperature so that the ITB and SFTs can have sufficient mobility in an appropriate simulation time.

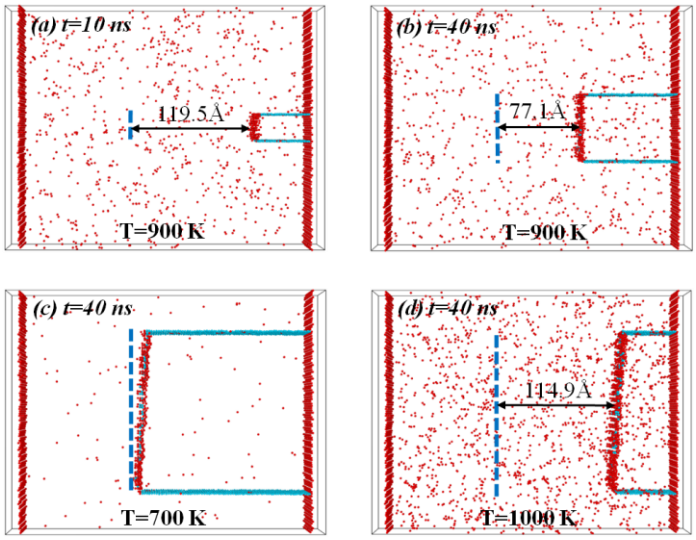

Figure 3 (a) ITB with 4 SUs annealed at 900 K for 10 ns, (b) ITB with 10 SUs annealed at 900 K for 40 ns, (c) ITB with 24 SUs annealed at 700 K for 40 ns, and (d) ITB with 24 SUs annealed at 1000 K for 40 ns. Atoms with perfect fcc structures have been removed. The dotted blue line indicates the initial position of ITB.

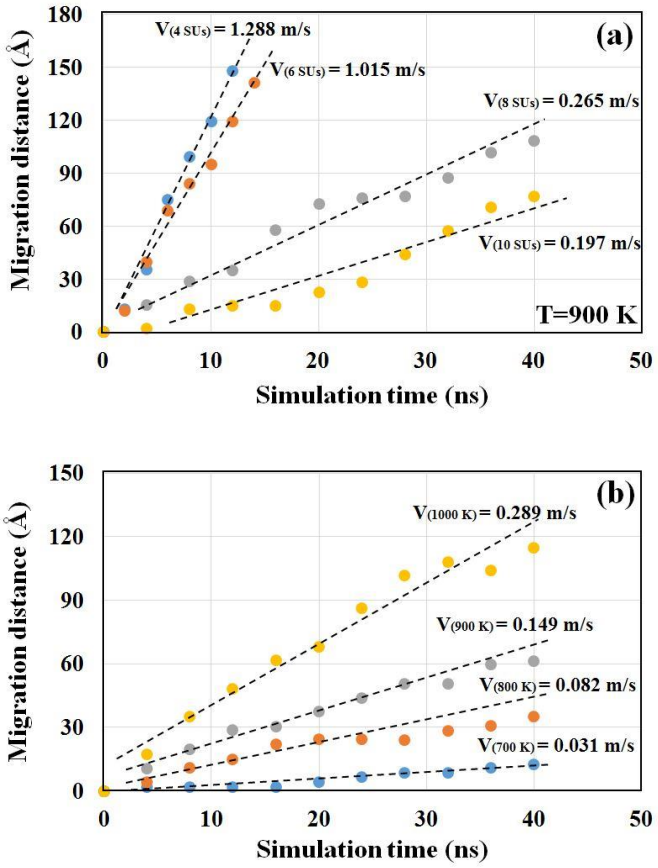

Figure 4 Migration distance of ITB as a function of the simulation time for (a) ITB with different length (n SUs) at 900 K, and (b) ITB with 24 SUs at different temperatures. The migration velocity was obtained by least-squares fitting.

3.2 Interaction of ITB and SFTs

Figure 5 shows the evolution of the CTB/ITB structure and the movement of the SFTs at different simulation time. The initial configuration of the simulation sample is shown in Fig.5(a). To clearly show the location of the twin boundaries and the SFTs, atoms with perfect fcc structure were removed, and the snapshots presented in Fig.5 were obtained after quenching back to 0 K at the corresponding simulation time (the following figures are displayed in the same manner). In Fig.5(b), the ITB migrated towards the right-hand side, while SFT-3 exhibited a random walk near its starting position and penetrated CTB-2 at t=10 ns. Subsequently, SFT-2 was completely absorbed by the migrating ITB after their interaction and SFT-1 crossed over CTB-1, as shown in Fig.5(c). By visual inspection of the MD result, the CTB structures are exactly the same as they were before the traversing of the SFTs, which implies that the interaction between the SFTs and CTBs was essentially negligible. In other words, a CTB does not act as a sink for an SFT as an ITB does. This is mainly due to the simplest boundary structure and the lowest boundary energy of the CTB among all the boundaries. Unlike the ITB, there are no misfit dislocations or free volumes present on the

boundary plane of a CTB. Moreover, the calculated interaction energy of a vacancy with a CTB is zero [10], indicating that the atomic distortion of a CTB is minimal. Therefore, a CTB cannot act as a sink nor as an obstacle to the movement of SFTs in the simulation. SFT-1 migrated near CTB-1 until it approached the ITB and was then annihilated at the CTB/ITB junction. The ITB continued to migrate after its absorption of SFT-1 and SFT-2, as shown in Fig.5(d) and (e). Meanwhile, SFT-3 moved towards ITB, and it was eventually absorbed by the migrating ITB in the same manner as SFT-1 and SFT-2. Fig.5(f) shows that all the three pre-existing SFTs were removed as the ITB swept. The dynamic process of Fig.5 is shown in the *supplementary movie-1*.

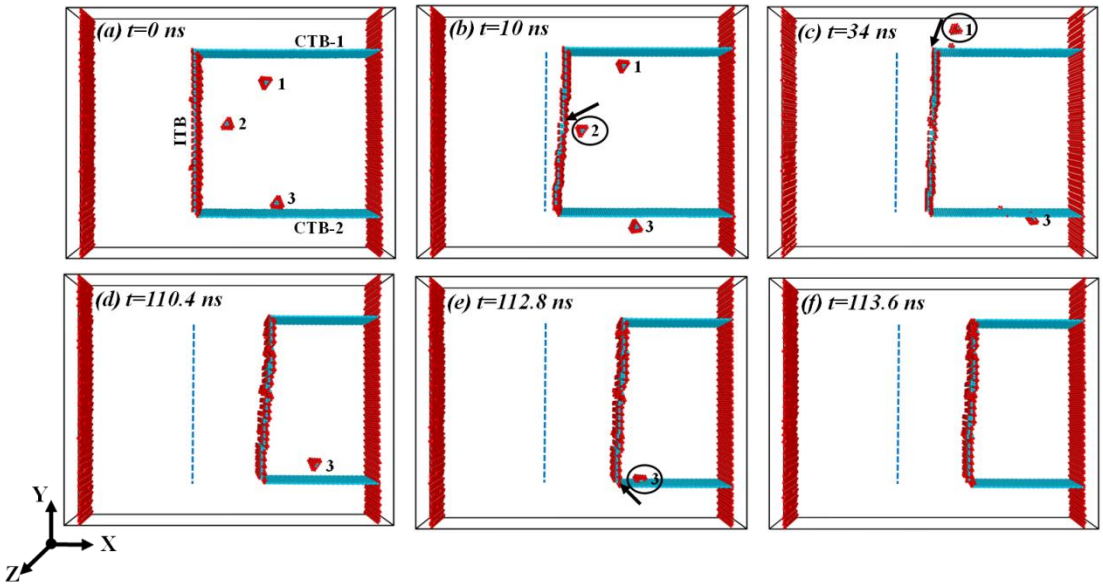

Figure 5 Movement of SFTs and their interactions with the CTB/ITB structure. The dimensions of the simulation sample are 295.2 Å×225.4 Å×40.8 Å (X×Y×Z). Atoms with perfect fcc structures have been removed. The dotted blue line indicates the initial position of ITB. (Movie-1 shows the dynamic process)

We found that the migration of the ITB did not change essentially after its absorption of SFTs. To examine the migration mechanism of the ITB before and after its absorption of SFT, Fig.6 shows the time progression of ITB migration at the atomic scale. For clarity, the cross-section views of the continues two layers of atoms along the <110> direction involved in the ITB-SFT interaction are presented. The initial ITB was flat and consisted of a line of rhombic SUs. To complete one step of the migration, the SUs must move a distance of an atomic layer along the <112> direction. However, the movement of SUs does not need to occur simultaneously on the whole boundary plane, and it first progressed in the SUs connected to the upper junction and then on the adjacent SUs, as shown in Fig.6(a) and (b). Also, the migration does not need to be completed throughout the boundary before the initiation of next boundary migration. The uncoordinated movement of the GB plane resulted in a number of steps or disconnections at the boundary plane, as indicated by the arrows. The migration process is very similar to the movement of the edge-type

dislocations in the Σ11{113} GB, which consist entirely of rhombic SUs [36], but the migration of the Σ11{113} GB was shear-driven while the motion of the ITB here was thermally activated. After the absorption of SFT-2, the essential structure of the ITB had not been changed, but the distance between the two Shockley partial dislocations had shortened, resulting in a step with a height of one atom, as shown by the dashed circle in Fig.6(c). The vacancies that dissociated from the SFT move along the boundary plane during the migration of the ITB, which was evidenced by the change in the position of the two adjacent Shockley partial dislocations in Fig.6(d).

The study case of the CTB/ITB structure can provide a good understanding of the experimental observations. For example, while the frequent migration of CTBs and ITBs was reported in irradiated nanotwinned Ag [12], our simulations indicate that the migration of ITBs is the predominant factor causing the removal of the SFTs rather than the CTB-SFT interaction mechanism. Also, the simulation result can explain the results of the *in situ* observation of the irradiated Cu films [25], where the radiation-induced defects were uniformly distributed in the region without the migration of an ITB, but the region with the ITB migration showed a lower defect density.

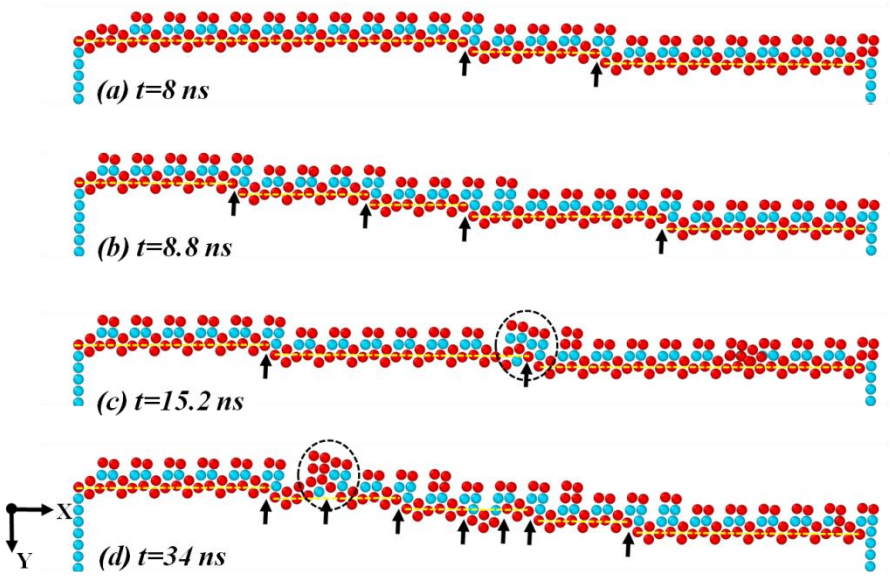

Figure 6 Migration mechanism of ITB. (a)-(b) Snapshots taken before the interaction with an SFT, (c)-(d) Snapshots taken after the absorption of SFT-2. The arrows indicate the disconnections or steps on the boundary plane. The dotted circles highlight the change in the local boundary structure due to the incoming vacancies.

3.3 Interaction of perfect CTB with SFTs and SIAs

Previous computational and experimental studies have shown that (i) a large number of vacancies and SIAs are generated in metals during heavy ion-irradiation [25, 37]; (ii) GBs can serve as an efficient sink to absorb radiation-induced point defects via different mechanisms [26, 38]; (iii) SIAs diffuse to GBs much faster than vacancies and are rapidly removed from grain interiors [26, 39], while the vacancy clusters generally take the form of SFTs inside the

grains [12, 40, 41]. Therefore, it is instructive to investigate the interaction between point defects and CTB incorporated with SIAs, because whether the defective CTB can provide the absorption site and diffusion channel that favor the annihilation of defects is not clear. To figure it out, the simulations were designed to be carried out in two steps. Firstly, we investigated the interaction of CTB with SFTs and SIAs, respectively.

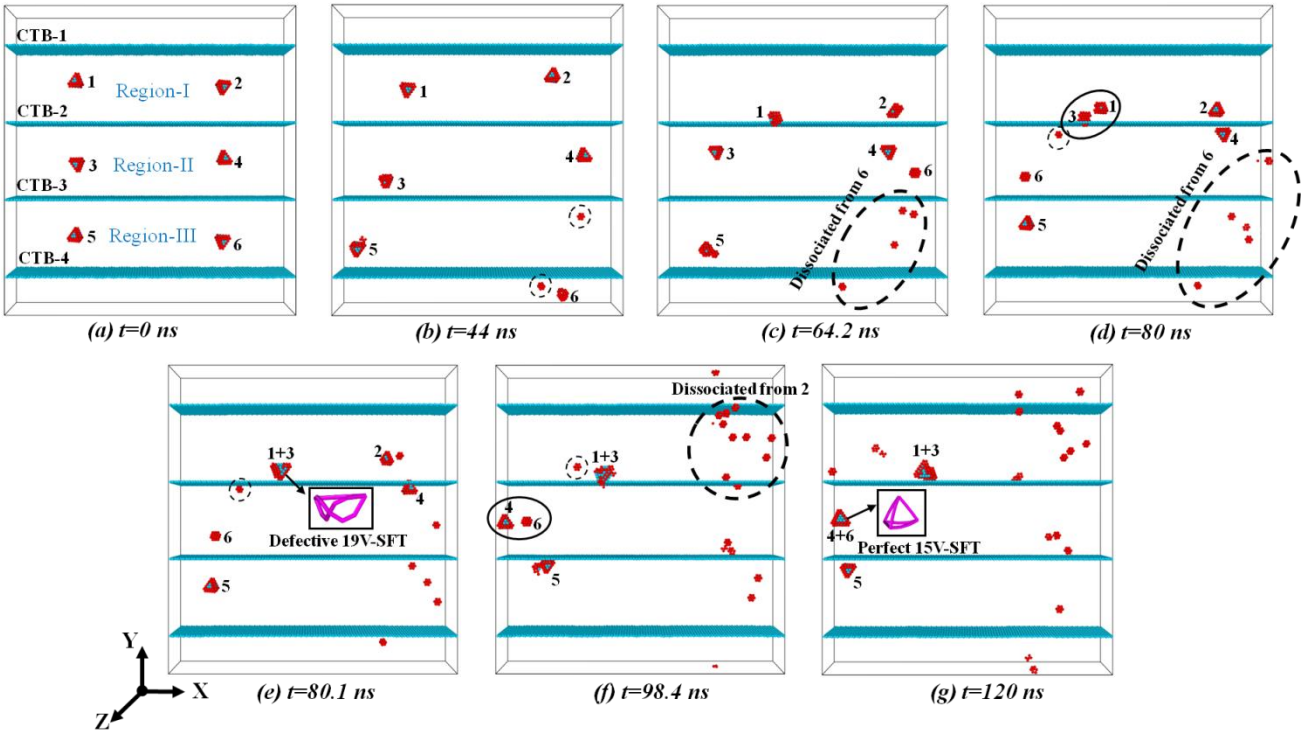

Figure 7 Movement of SFTs and their interaction with CTBs at different simulation time. The dimensions of the sample are 234.6 Å×250.4 Å×40.8 Å (X×Y×Z). Atoms with perfect fcc structures have been removed.

Selected snapshots of the interaction between CTBs and SFTs are presented in Fig.7. The SFTs changed their equilibrium configuration and moved randomly between the twin lamellas during the high-temperature annealing. For example, SFT-6 crossed CTB-4 at t=44 ns and then traversed CTB-4 and CTB-3 continuously to reach region II at t=64.2 ns, as shown in Figs.7(b) and (c). During the migration of SFT-6, five vacancies were dissociated from its main body, as indicated by the dashed ellipse in Fig.7(d). SFT-6 has now transformed to a void structure and was unable to change back to an SFT unless new vacancies were absorbed, because the minimum number of vacancies required to form an SFT is six. Meanwhile, SFT-3 crossed CTB-2 to reach region I and moved close to SFT-1, but only one vacancy was separated. Subsequently, SFT-1 and SFT-3 merged to form a larger size SFT containing 19 vacancies, as shown in Fig.7(e). Note that the newly generated SFT had a defective tetrahedron structure because the number of vacancies required to form a perfect tetrahedron of the same size is 21. As shown in Fig.7(f), SFT-4 moved near void-6 and they subsequently combined to form a perfect SFT containing 15 vacancies, while for SFT-2,

complete dissociation to 10 vacancies was observed, as shown by the dashed circle. The defective 19V-SFT and the perfect 15V-SFT structures were identified by the dislocation extraction algorithm (DXA) [42, 43], as shown by the purple lines in Figs.7(e) and (g), and were made up entirely of 1/6<110> strair-rod dislocations. The final products of the CTB-SFT interaction at t=120 ns include SFTs with different sizes, a group of dissociated vacancies between the twin lamellas, and the intact CTBs.

Fig.8 shows the interaction between the CTBs and SIAs at different simulation time. The SIAs show higher mobility than the SFTs, and they immediately aggregate to form dislocation-loop-like-interstitial clusters inside the grain, as shown in Fig.8(b) and (c), where the atomistic view and the DXA result are presented. The main result of the CTBs-SIAs interaction discovered here is that CTBs absorb interstitials preferentially over vacancies, and all the preexisting bulk interstitials were eventually arranged in twin boundary planes in the form of self-interstitial clusters. These SIA clusters can be described as closed-loop line defects, as shown in Figs.8(d) and (e). In summary, the above simulations indicate that the interaction between the CTBs and the vacancy-type defects (including monovacancies, voids and SFTs) is not sufficient to absorb the defects or keep them bound to the CTBs, while for the interstitial atoms, they can aggregate at CTBs in a short time and change the perfect CTB structure into a locally defective one.

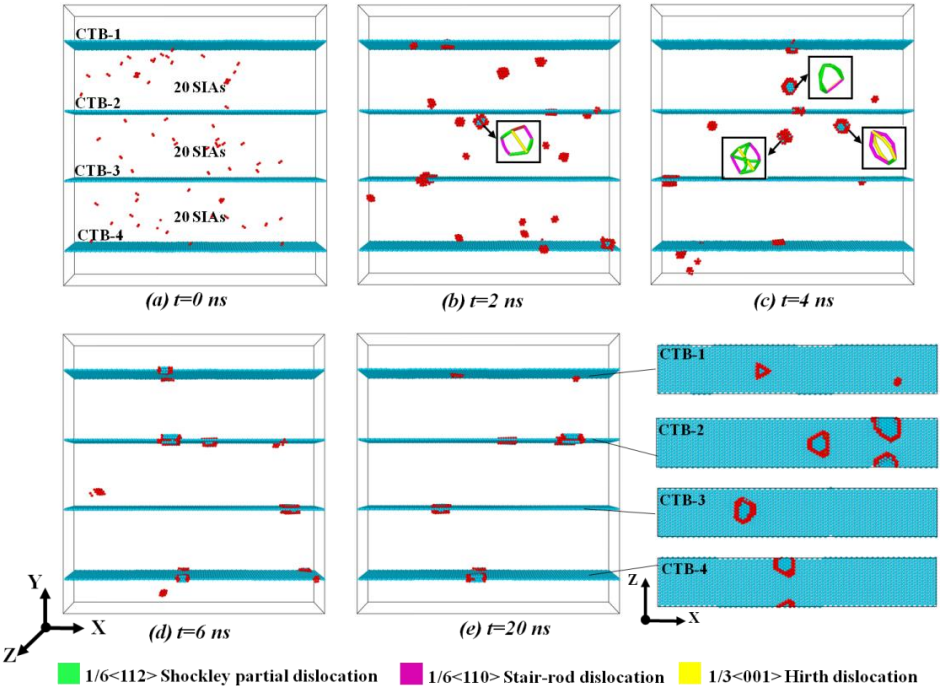

Figure 8 Movement of SIAs and their interaction with CTBs at different simulation time. Atoms with perfect fcc structures have been removed. The colored lines are the dislocations indentified by DXA.

3.4 Interaction of defective CTB with SFTs

We follow the next study on the role the defective CTB structure plays in the absorption of SFTs. To exclude any

interaction of SIAs and SFTs between the twin lamellas, the SFTs in Fig.7(a) were directly introduced into the defective CTBs in Fig.8(e). The simulation was performed under the same conditions as those in the first step, and the results are shown in Fig.9. Similarly, the SFTs transformed their perfect structure into a void-like configuration during high-temperature annealing and exhibited a random walk. Meanwhile, the SIA clusters slipped on the twin boundary plane, and they can grow by combining with other SIAs. In Fig.9(a2) and (a3), it is interesting to see that the defective twin boundary at S2 was recovered when SFT-1 and SFT-2 moved close to S2 and were absorbed by it. A similar event was also observed on CTB-3. When slipping on CTB-3, the size of S4 was reduced by its interaction with SFT-3, and it was completely removed after its combination with SFT-5, as shown in Fig.9(a3) to (a5). In a similar way, the size of S4 was reduced as a result of absorbing the surrounding distributed vacancies from t=29.2 ns to t=84 ns. Although the simulation was performed for a limited time, the remaining vacancies and their clusters in Fig.9(a6) are significantly smaller than those in the initial state. Fig.9(b) and (c) show bottom views of the evolution of CTB-2 and CTB-3, respectively, during the simulation. It can be clearly seen that the defective CTB structures at S2 and S4 were completely recovered and the size of S3 was reduced. The dynamic process of Fig.9 is shown in the *supplementary movie-2*. It is expected that all the remaining vacancy defects between the twin lamellas would have been removed and that the defective CTB structures would have been completely recovered if the simulation had been performed for a sufficiently long time. The simulation result implies that the ability of the CTBs to act as a sink for vacancy defects was significantly improved after their absorption of interstitial atoms. In a real situation, the continuous segregation of SIAs at CTBs can provide sufficient absorption sites to accommodate the vacancies and their clusters inside grains. Therefore, the switching back and forth between perfect and the defective coherent twin structures allows CTBs to be an efficient sink for radiation-induced point defects.

4 Conclusion

In conclusion, we investigated the ability of twin boundaries to act as a sink for point defects by performing molecular dynamics simulations. Most of the simulations in this study were carried out at 100 ns time scale which is rarely accessed by the previous MD simulations. The long-time simulation makes it possible to study the dynamic motion of the point defects and their interaction with twin boundaries. In particularly, the defective CTB structures which contain ITB segment or self-interstitial atoms were considered in this study; such kind of CTB structures are more close to the experimental observations and the actual situation. The simulation results show that while a perfect CTB was ineffective for absorbing SFTs, a defective CTB structure containing ITB segments can provide a preferential site and diffusion channel to remove them. In addition, the absorption process of the point defects can be accelerated

by the migration of ITB between the CTB lamellas. CTBs absorb SIAs preferentially over vacancies, and the SIAs exist on CTBs in the form of dislocation-loop-like interstitial clusters. The SIA clusters on CTBs can subsequently provide absorption sites that favor the annihilation of vacancies inside grains. This study gives a good explanation for recent experimental findings at the atomic scale and provides further support for the design of radiation-tolerant nanotwinned materials.

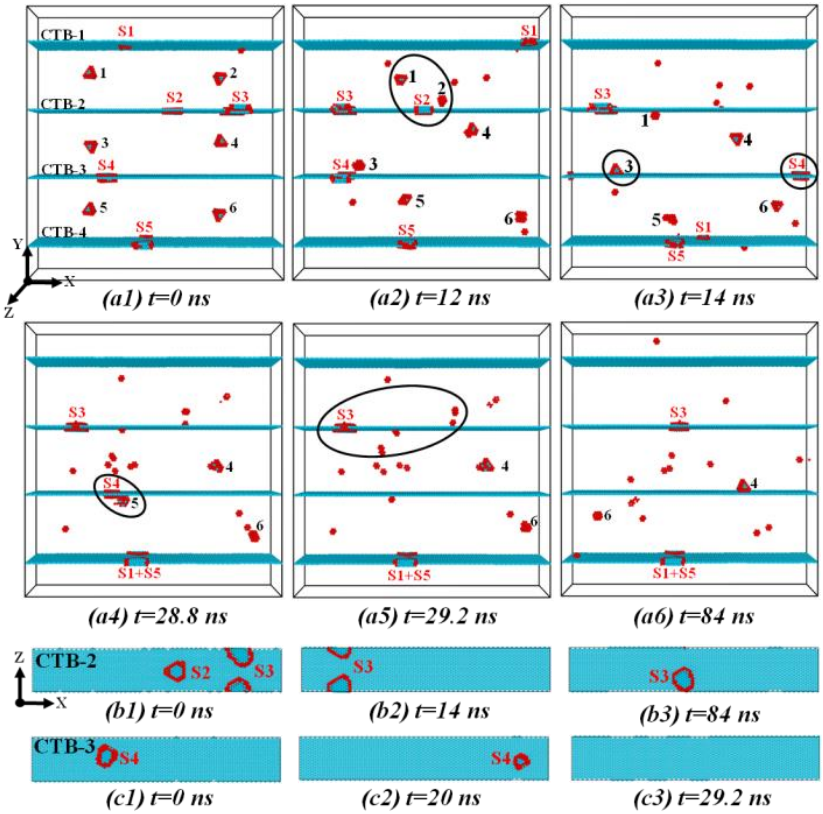

Figure 9 (a) Movement of SFTs and their interactions with defective CTBs. The SFTs are indexed from 1 to 6, and the SIA clusters on the CTBs are indexed from S1 to S6. Atoms in fcc environment were removed. (b)-(c) Bottom views of CTB-2 and CTB-3. (Movie-2 shows the dynamic process)

Acknowledgement

Liang Zhang would like to acknowledge the Postdoctoral Fellowship Program (P17711) awarded by Japan Society for the Promotion of Science (JSPS) and Australian Academy of Science (AAS). This work was supported by the Grand-in-Aid for JSPS Fellows (17F17711) and the Australian Research Council Discovery Project (DP170103092).

References

[1] K.S. Kumar, H. Van Swygenhoven, S. Suresh. Acta Mater. 51 (2003) 5743-5774.

[2] M.A. Meyers, A. Mishra, D.J. Benson. Prog. Mater. Sci. 51 (2006) 427-556.

[3] M. Dao, L. Lu, R.J. Asaro, J.T.M. De Hosson, E. Ma. Acta Mater. 55 (2007) 4041-4065.

[4] L. Lu, Y. Shen, X. Chen, L. Qian, K. Lu. Science 304 (2004) 422-426.
[5] L. Lu, X. Chen, X. Huang, K. Lu. Science 323 (2009) 607-610.
[6] X. Zhang, A. Misra, H. Wang, M. Nastasi, J.D. Embury, T.E. Mitchell, R.G. Hoagland, J.P. Hirth. Appl. Phys. Lett. 84 (2004) 1096-1098.
[7] M.J. Demkowicz, O. Anderoglu, X. Zhang, A. Misra. J. Mater. Res. 26 (2011) 1666-1675.
[8] W.Z. Han, M.J. Demkowicz, E.G. Fu, Y.Q. Wang, A. Misra. Acta Mater. 60 (2012) 6341-6351.
[9] X.M. Bai, L.J. Vernon, R.G. Hoagland, A.F. Voter, M. Nastasi, B.P. Uberuaga. Phys. Rev. B 85 (2012) 214103.
[10] E. Martínez, B.P. Uberuaga, I.J. Beyerlein. Phys. Rev. B 93 (2016) 054105.
[11] X. Zhang, K. Hattar, Y. Chen, L. Shao, J. Li, C. Sun, K. Yu, N. Li, M.L. Taheri, H. Wang, J. Wang, M. Nastasi. Prog. Mater. Sci. 96 (2018) 217-321.
[12] K.Y. Yu, D. Bufford, C. Sun, Y. Liu, H. Wang, M.A. Kirk, M. Li, X. Zhang. Nat. Commun. 4 (2013) 1377.
[13] Y. Chen, J. Li, K.Y. Yu, H. Wang, M.A. Kirk, M. Li, X. Zhang. Acta Mater. 111 (2016) 148-156.
[14] Y. Chen, K.Y. Yu, Y. Liu, S. Shao, H. Wang, M.A. Kirk, J. Wang, X. Zhang. Nat. Commun. 6 (2015) 7036.
[15] J. Li, K.Y. Yu, Y. Chen, M. Song, H. Wang, M.A. Kirk, M. Li, X. Zhang. Nano Lett. 15 (2015) 2922-2927.
[16] L. Pei, C. Lu, X. Zhao, L. Zhang, K. Cheng, G. Michal, K. Tieu. Acta Mater. 89 (2015) 1-13.
[17] X. Zhao, C. Lu, A.K. Tieu, L. Pei, L. Zhang, K. Cheng, M. Huang. Mater. Sci. Eng. A 676 (2016) 474-486.
[18] X. Zhao, C. Lu, A.K. Tieu, L.Q. Pei, L. Zhang, L.H. Su, L.H. Zhan. Mater. Sci. Eng. A 687 (2017) 343-351.
[19] Z.H. Jin, P. Gumbsch, K. Albe, E. Ma, K. Lu, H. Gleiter, H. Hahn. Acta Mater. 56 (2008) 1126-1135.
[20] Y.M. Wang, F. Sansoz, T. LaGrange, R.T. Ott, J. Marian, T.W. Barbee, A.V. Hamza. Nat. Mater. 12 (2013) 697-702.
[21] J.R. Greer. Nat. Mater. 12 (2013) 689-690.
[22] L. Xu, D. Xu, K.N. Tu, Y. Cai, N. Wang, P. Dixit, J.H.L. Pang, J.M. Miao. J. Appl. Phys. 104 (2008) 113717.
[23] J.A. Brown, N.M. Ghoniem. Acta Mater. 57 (2009) 4454-4462.
[24] J. Wang, N. Li, O. Anderoglu, X. Zhang, A. Misra, J.Y. Huang, J.P. Hirth. Acta Mater. 58 (2010) 2262-2270.
[25] N. Li, J. Wang, Y.Q. Wang, Y. Serruys, M. Nastasi, A. Misra. J. Appl. Phys. 113 (2013) 023508.
[26] X.M. Bai, A.F. Voter, R.G. Hoagland, M. Nastasi, B.P. Uberuaga. Science 327 (2010) 1631-1634.
[27] X.M. Bai, B.P. Uberuaga. JOM 65 (2013) 360-373.
[28] X. Li, W. Liu, Y. Xu, C.S. Liu, B.C. Pan, Y. Liang, Q.F. Fang, J.-L. Chen, G.N. Luo, G.-H. Lu, Z. Wang. Acta Mater. 109 (2016) 115-127.
[29] S. Plimpton. J. Comp. Phys. 117 (1995) 1-19.
[30] Y. Mishin, M.J. Mehl, D.A. Papaconstantopoulos, A.F. Voter, J.D. Kress. Phys. Rev. B 63 (2001) 2241061-22410616.
[31] M.H. Loretto, P.J. Phillips, M.J. Mills. Scr. Mater. 94 (2015) 1-4.
[32] L. Zhang, C. Lu, G. Michal, G. Deng, K. Tieu. Scr. Mater. 136 (2017) 78-82.
[33] L. Zhang, C. Lu, K. Tieu, L. Su, X. Zhao, L. Pei. Mater. Sci. Eng. A 680 (2017) 27-38.
[34] E.A. Marquis, J.C. Hamilton, D.L. Medlin, F. Leonard. Phys. Rev. Lett. 93 (2004) 156101.
[35] E. Martinez, B.P. Uberuaga. Sci. Rep. 5 (2015) 9084.
[36] L. Zhang, C. Lu, K. Tieu, X. Zhao, L. Pei. Nanoscale 7 (2015) 7224-7233.
[37] K.Y. Yu, D. Bufford, F. Khatkhatay, H. Wang, M.A. Kirk, X. Zhang. Scr. Mater. 69 (2013) 385-388.
[38] L. Zhang, C. Lu, K. Tieu, Y. Shibuta. Scr. Mater. 144 (2018) 78-83.
[39] M.A. Tschopp, K.N. Solanki, F. Gao, X. Sun, M.A. Khaleel, M.F. Horstemeyer. Phys. Rev. B 85 (2012) 064108.
[40] B.N. Singh, S.J. Zinkle. J. Nucl. Mater. 206 (1993) 212-229.
[41] R. Schäublin, Z. Yao, N. Baluc, M. Victoria. Philos. Mag. 85 (2005) 769-777.
[42] A. Stukowski. Model. Simul. Mater. Sci. Eng. 20 (2012) 045021.
[43] A. Stukowski, K. Albe. Model. Simul. Mater. Sci. Eng. 18 (2010) 025016.